J Fluoresc (2008) 18:17–27
DOI 10.1007/s10895-007-0229-6

ORIGINAL PAPER

Temperature-dependent Time-resolved Fluorescence Study of Cinchonine Alkaloid Dication

Hirdyesh Mishra · Sanjay Pant · Hera B. Tripathi

Received: 30 May 2007 / Accepted: 17 July 2007 / Published online: 23 August 2007

Abstract Photo induced excited state dynamical processes of cinchonine alkaloid dication (C^{++}) have been studied over a wide range of temperature using steady state and nanosecond time-resolved fluorescence spectroscopic techniques. The temperature-dependent fluorescence studies of C^{++} clearly indicate the existence of two distinct emitting species having their own characteristic decay rates. The shorter-lived species shows a usual temperature dependence with increasing non-radiative deactivation at higher temperatures, while the longer-lived species show features resembling to the excited state solvent relaxation process with a large solvent relaxation time (τ_r~6 ns). The species emitting in the lower energy side, having longer decay time is found to be more sensitive towards chloride ion quenching and has a charge transfer character. Further, concentration quenching with decrease in τ_r of long lived species shows the possibility of energy migration along with solvent relaxation in C^{++}.

Keywords Cinchonine · Solvent relaxation · Fluorescence quenching

Introduction

Photo-physics and photochemistry of cinchona alkaloid systems is a matter of great interest because of its possibility of developing new molecular structures for pharmacologically active compounds and in photosynthesis for biological system. It is also found to be very useful in environment monitoring, soft drinks etc. [1–8]. The study of the rigid structure of cinchona alkaloids is also excellent for stereo chemical analysis of photochemical reactions. Alkaloids quinine sulphate (QS), quinidine (Qd), cinchonine (C) and cinchonidine (Cd), are some of the basic members belonging to cinchona family. All these alkaloids are all made up of a quinoline ring (basic fluorophore unit) joined to a substituted chiral 1-azabicyclo [2.2.2] octane moiety through stereogenic carbon C9 [2]. But the fundamental difference is presence of methoxy group at the sixth position in QS and Qd, while it is absent in C and Cd. The pairs QS, Qd and C, Cd are also termed as pseudo-enantiomeric. The doubly-charged cations of these compounds derived from acidified aqueous solutions (1 N H_2SO_4) have been used because of the high photo stability and having good fluorescence quantum yield [9].

The time-resolved fluorescence spectroscopy has provided valuable information regarding the photophysical phenomena associated with the excited state interactions and relaxation processes. Fluorescence emission normally occurs on a nanosecond time scale, whereas the relaxation of polar solvent molecules around the changed dipole moment of the excited state occurs in pico-second time scale in the fluid media. However, in dication of quinine sulphate (QS^{++}), quinidine (Qd^{++}) and 6-methoxyquinine ($6MQ^{+}$), the excited state solvent relaxation occurs on a nanosecond time scale even at ambient temperature [9–13]. Itoh and Azumi [14] investigated QS at room temperature in detail and interpreted their results on the basis of solvent relaxation process. O'Connor et al. [15] observed the time dependent fluorescence Stoke's shift (TDFSS) for QS in 1 N H_2SO_4 (water) solution. The presence of TDFSS is due

H. Mishra
Molecular Biophysics Unit, Indian Institute of Science,
Bangalore 560012, India

H. Mishra (✉) · S. Pant · H. B. Tripathi
Photophysics Laboratory, Department of Physics,
Kumaun University,
Nainital 263001, India
e-mail: hirdyesh@mbu.iisc.ernet.in

to a relaxation from a Franck–Condon to an equilibrium state [16–20]. For TDFSS to occur the solvent relaxation time τ_r should compete with the fluorescence decay time τ_F [21]. Ikeyama et al. [22] suggested that one should be able to observe a TDFSS for a fluid solution which exhibits edge excitation red shift (EERS). From, the temperature variation studies of fluorescence decay time of acidic QS, Meech et al. [23] concluded that, at least some of the configurations that have short excited state decay times are somewhat isolated from other states, whereas some may interconvert freely with the longer-lived conformations to show a rise time.

Earlier TDFSS in QS^{++}, Qd^{++} and $6MQ^{+}$ [9–13] had been studied extensively and it has been found that all these three compounds show a similar behavior. The study showed that the methoxy group plays an important role in the photophysics of these molecules. In the decay analysis the longer-lived (τ_2) component is due to the charge transfer (CT) state modified by solvent relaxation and the shorter-lived (τ_1) component is due to the original state which gives rise to the CT state. TDFSS in these compounds is explained fairly well in accordance with the Bakhshiev formulation [16–18] of solvent relaxation. The two major relaxation processes in these molecules has been suggested, an accelerated charge transfer (CT) around 160 K and the solvent relaxation in polar fluid media [9]. Although, there are similarities between the two relaxation processes occurring in the excited state of the three protonated methoxy quinoline derivatives, but still there are some differences in their fluorescence kinetic parameters. Moreover, the complexities in their photophysics as well as in the conformational changes in the ground state under similar environmental conditions differ in these alkaloids [24]. Further, the temperature dependence of the decay time of QS^{++} and Qd^{++} shows an unusual behavior for the longer decay time component at low temperatures. The photophysics of their parent compounds cinconine (C^{++}) and cinchonidine (Cd^{++}) at room temperature shows absence of rise time at longer wavelength unlike QS^{++} and Qd^{++} [25]. Recently, the time domain fluorescence and 2D NMR study of complexation of cinchona alkaloids have been reported by Lue et al. [26]. It was observed that there is no change in fluorescence parameters of cinchonine with complexation of β-cyclodextrin. The absence of hydrogen bonding interaction in these chiral tether molecules was also reported. The chemical structure of C^{++} molecule is shown in Fig. 1.

From the above discussion it is evident that the photophysics of these alkaloids is quite complex. In order to gain further insight into this complexity, we have undertaken the fluorescence steady state and time-resolved studies of C^{++} at different temperatures.

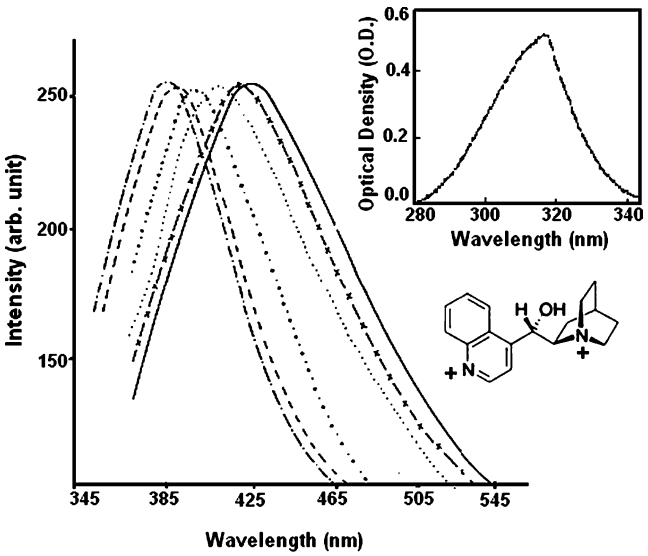

Fig. 1 Emission spectra of C^{++} in glycerol/water (1:1) system; at 80 K (–·–·–), 200 K (–), 240 K (+·+·+·+) 250 K (·····), 270 K (x–x–x–x), 295 K (—); λ_{ex}=320 nm. (Absorption spectra of C^{++} at a concentration of approximately 10^{-4} M in glycerol/water shown in *inset*)

Experimental

Material

Cinchonine (obtained from Aldrich) was re-crystallized from an aqueous solution. All the solvents used were either of spectroscopic grades or were checked for their fluorescence purity. Triply distilled water was used in these experiments. All the samples of C^{++} were prepared by dissolving an appropriate concentration of cinchonine in 1N H_2SO_4 containing HPLC grade water (SRL SISCO laboratory chemicals).

Steady state measurements

The absorption spectra, at room temperature were recorded using Beckman DU-70 and JASCO V-550 spectrophotometer. The emission and excitation spectra were recorded with JASCO FP-777 and an indigenously designed spectrofluorometer, consisting of a HRS-2 monochromator for scanning fluorescence emission. Low temperature measurements were carried out using liquid nitrogen in a quartz jacket.

Time domain measurements

Fluorescence decay times and time-resolved emission spectra were recorded using Edinburgh Instrument (EI) FLA-199 time domain spectrometer and analyzed by related software. The excitation source was a hydrogen

gas filled thyratron gated nanosecond flash lamp. Lamp profile was measured at the excitation wavelength using Ludox scatter. The head on photomultiplier tube (PMT) XP2020x was used as detector. In the lamp profile a second peak was observed, after 14 ns from main excitation pulse due to secondary emission photon of the transparent cathode of the PMT. The pulse width was about 1.0 ns with repetition rate of 20 KHz. The decay times was determined using non-linear least square method by time correlated single photon counting (TCSPC) technique. Care was taken in data analysis to differentiate between the mono-exponential and bi-exponential fits by judging the χ^2 values, standard deviations and weighted residuals. Intensity decay curves so obtained were fitted to sum of exponential terms as:

$$I(\tau, t) = \alpha_1 \exp^{-t/\tau_1} \pm \alpha_2 \exp^{-t/\tau_2} \quad (1)$$

where τ_1 and τ_2 are the shorter and longer decay time components respectively, α_1 and α_2 are the corresponding amplitudes in C^{++}. The negative sign indicates the rise time at the red edge of the emission of the C^{++}. The average decay time $<\tau>$ for bi-exponential decays of fluorescence was calculated from the observed decay times (τ_1, τ_2) and pre-exponential factors (α_1, α_2) using the following equation:

$$\langle \tau \rangle = \frac{\alpha_1 \tau_1^2 + \alpha_2 \tau_2^2}{\alpha_1 \tau_1 + \alpha_2 \tau_2} \quad (2)$$

The time-resolved emission spectra (TRES) were also obtained with the help of EI-FLA-199. For TRES measurements the TAC (time to amplitude converter) is bypassed, and signal from the discriminator, on the emission channel, is routed directly to the multi-channel analyzer (MCA) in single channel analyzer mode. With the channel advance rate synchronized with the wavelength drive of the emission monochromator, the resulting histogram represents the fluorescence spectrum of the sample. The single channel analyzer (SCA) is essentially a timing discriminator with two variable levels, V_L and V_U. Input pulses having amplitude lower than V_L and higher than V_U are rejected. Spectra were recorded by using the above method, after a certain time delay Δt, within a time window δt, selected by upper level discriminator (ULD) and lower level discriminator (LLD). Photons in discrete time intervals are summed up and arranged as a function of wavelengths. Measurements at various temperatures were carried out using a Eurotherm temperature controller (available with the EI-FLA-199 spectrometer) and liquid nitrogen in a quartz jacket. A transparent Dewar flask was placed in the sample compartment and the samples were immersed in liquid air. The instrumental profile was obtained in this case at the excitation wavelength in the same geometry as used for fluorescence decay. The temperature variations were recorded with an iron-constantan thermocouple. The data presented here for temperatures below 0°C is accurate to within 5°C. Fluorescence quenching experiments were carried out by adding different concentrations of Cl^- ion in glycerol/water solution containing C^{++} ion.

Results and discussion

The absorption spectrum for C^{++} in [1N H_2SO_4] glycerol: water at concentration 10^{-4} M is given in Fig. 1 (inset) along with its molecular structure. The absorption peak at 316 nm resembles the long wavelength band of quinoline at 313 nm (L_a) along with a hump at 308 nm (L_b). The emission spectrum of C^{++} consists of broad spectrum with emission maxima at 425 nm, (using 305 nm excitation). The emission shows excitation wavelength dependence. The magnitude of edge excitation red shift (EERS) is found to be approximately 800 cm^{-1} (for aqueous solution) and approximately 1,548 cm^{-1} (for glycerol/water system), expressed as the difference between the emission maxima obtained at blue edge (305 nm) and red edge 365 nm excitations. The full width half maximum (FWHM) varies from 3,660 cm^{-1} to 5,500 cm^{-1} for the same range of excitation wavelength.

The time domain measurements of C^{++} in 1N H_2SO_4 solution of glycerol/water, exhibited a dual exponential decay throughout the emission profile as shown in Fig. 2. Standard deviation corresponding to the distribution of residuals for single and double exponential fits are given above and below the decay curves respectively. It appears that shorter decay time (τ_1) value remains almost constant across the emission wavelength while the longer decay time value (τ_2) increases as shown in Table 1. The amplitudes α_1 and α_2 are positive throughout the emission wavelength indicating the existence of emission from two different conformers. The amplitude I_1 (corresponding to τ_1) decreases while I_2 (corresponding to τ_2) increases with increasing emission wavelength. The fluorescence quantum yield (ϕ) of C^{++} at various emission wavelengths has been calculated with the help of following equation [27]:

$$\phi = \left(\frac{\alpha_1 \tau_1 + \alpha_2 \tau_2}{\alpha_1 + \alpha_2} \right) \tau_{rad}^{-1} \quad (3)$$

where τ_{rad}. is the calculated radiative decay time and it has been calculated from well known Stickler and Berg relation [28]; using the absorption and emission spectra and extinction coefficient for 10^{-4} M aqueous solution of C^{++}. This comes out to be 19.15 ns. The value of ϕ is found to increase with the increase in emission wavelength (Table 1) indicating longer decay time species (emitting towards red

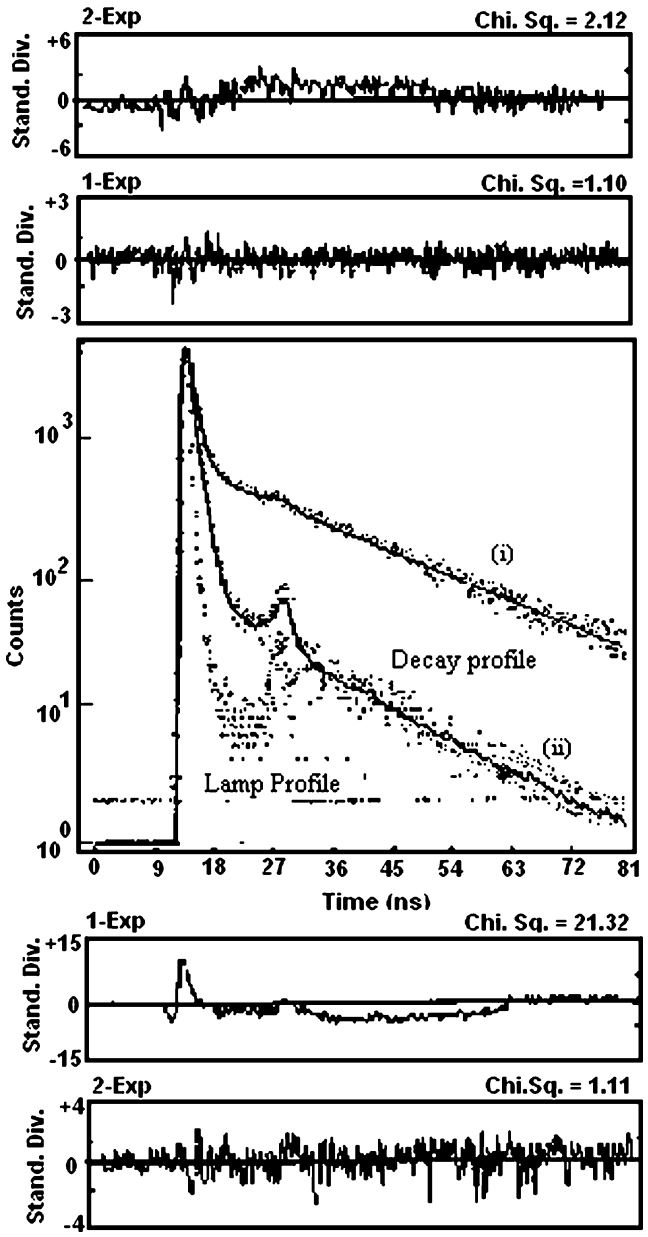

Fig. 2 Fluorescence decay curve of C^{++} in glycerol/water (1:1) system, at 294 K fitted to a double exponential function for (*i*) λ_{em}= 360 nm and (*ii*) λ_{em}=490 nm (λ_{ex}=320 nm). Distributions of residuals and χ^2 shows above and below for single and double exponential fit respectively

side of the emission band) shows high quantum yield with respect to shorter decay time species.

Temperature effects

Investigation of effect of temperature on both the steady state and time dependent fluorescence parameters has been carried out for C^{++} in glycerol/water (1:1) solvent from 80 to 294 K. Figure 1 depicts the temperature variation for the fluorescence spectrum. The fluorescence spectrum at 80 K with λ_{max}~381 nm shows a large red shift with λ_{max}~ 421 nm at room temperature. The fluorescence at 80 K with λ_{max}~381 shows a large red shift with λ_{max}~421 at room temperature. Figure 3 and Table 2 show the temperature variation of fluorescence maxima $\overline{\nu}_{max}$ and full width half maximum (FWHM) of the emission. While $\overline{\nu}_{max}$ shows a sudden decrease (i.e., a red shift in the fluorescence spectrum) around 200 K, FWHM shows an increase beyond this temperature. An increase of approximately 710 cm^{-1} in FWHM and a red shift in fluorescence spectrum of approximately 2,490 cm^{-1} is observed with increase in temperature from 80 to 294 K. This type of behavior is attributed to the solvent relaxation processes around the fluorophores, which undergo a significant change of charge distribution on electronic excitation. At 80 K such solvent relaxation processes are frozen out and hence the spectrum is blue shifted. However, at temperatures around which orientational relaxation takes place, the total fluorescence spectrum is composed of many spectra originating from various species having different solvent orientations. Hence an increase in FWHM and a red shift is observed. Since, the onset of the sudden change in $\overline{\nu}_{max}$ and FWHM takes place around 200 K, (where such solvent motions are slowed down), the possibility of the molecule undergoing a geometrical change cannot be ruled out. However, in fluid solutions the existence of solvent reorientation process is clearly depicted by time-resolved spectroscopy.

The low temperature decay measured at 420 nm (λ_{ex}= 320 nm) shows a double exponential behavior. The temperature variation of the decay times (τ_1 and τ_2) is

Table 1 Time domain parameters of cinchonine alkaloid (concentration 1×10^{-4} M) in 1 N H_2SO_4 glycerol/water (1:1) system at different emission wavelengths

λ_{em} (nm)	τ_1 (ns)	τ_2 (ns)	α_1	α_2	χ^2	$<\tau>$	ϕ	$I_1=\frac{\alpha_1\tau_1}{\alpha_1\tau_1+\alpha_2\tau_2}$	$I_2=\frac{\alpha_2\tau_2}{\alpha_1\tau_1+\alpha_2\tau_2}$
390	1.13±0.02	17.16±0.10	0.251	0.035	1.10	2.38	0.16	0.3208	0.6792
420	1.34±0.04	18.02±0.07	0.157	0.073	1.15	5.92	0.31	0.1379	0.8621
450	1.43±0.07	18.89±0.06	0.116	0.106	1.25	9.18	0.48	0.0765	0.9235
480	1.33±0.08	19.29±0.05	0.075	0.122	1.22	12.81	0.66	0.0407	0.9593
510	1.26±0.09	19.59±0.05	0.069	0.128	1.11	12.91	0.67	0.0335	0.9665

(λ_{ex}=320 nm and temperature 294 K)

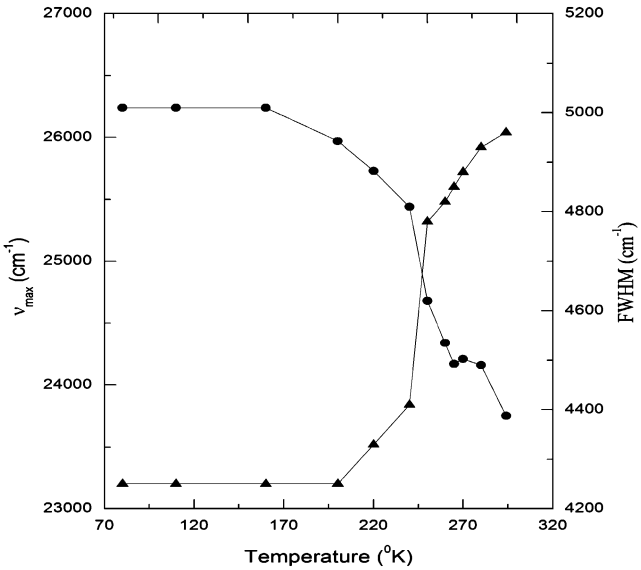

Fig. 3 Curve of emission maximum (ν_{max}) and FWHM against temperature of C^{++} in glycerol/water (1:1) system (λ_{ex}=320 nm)

given in Fig. 4 (Table 3). The decay curves exhibit a double exponential nature at all the temperatures measured between 80 and 294 K. At 80 K the contribution of τ_1 and τ_2 components to the total intensity is roughly 54% and 46%, respectively. The values of decay times τ_1 and τ_2 are almost constant upto 200 K, however, these parameters show a gradual but significant decrease beyond this temperature. As is evident from Fig. 4, there is a decrease in τ_1 at temperature around 240 K, while τ_2 shows a relatively gradual decrease with increasing temperature. The amplitude of the small decay time component (α_1) decreases from 80 to 200 K, beyond which it again shows a steady increase. The amplitude of the longer decay time component (α_2) increases with temperature, although not linearly. These changes in relative amplitudes (α_1 and α_2) are obviously due to the shift in the emission spectrum around 220 K (Fig. 3). The relative intensity values I_1 and I_2

Table 2 Steady state parameters of cinchonine alkaloid in 1 N H_2SO_4 glycerol/water (1:1) system at different temperatures (λ_{ex}=320 nm)

Temperature (K)	λ_{em} max (cm^{-1})	FWHM (cm^{-1})
80	26,240	4,250
110	26,240	4,250
160	26,240	4,250
200	25,970	4,250
220	25,730	4,330
240	25,440	4,410
250	24,680	4,780
260	24,340	4,820
265	24,170	4,850
270	24,210	4,880
280	24,160	4,930
294	23,750	4,960

(corresponding to emitting species having decay time τ_1 and τ_2 respectively) have been calculated from the decay associated parameters at different temperatures for emission wavelength 420 nm (given in Table 3). Plot of I_1 and I_2 with temperature is given in Fig. 4 which shows a decrease of I_1 and increase of I_2 with increasing temperature. We expected a change of I_1 similar to τ_1 with temperature. But, since the emission spectrum shows a temperature-dependent red shift, the values of I_1 calculated at different temperatures for the same emission wavelength will give uncorrected value of I_1. Thus, we observe a discontinuity in the I_1 vs temperature curve. Further, decrease of I_2 with decrease in temperature is assigned to a decrease in the percentage of CT species. As a consequence the molecules at low temperature are trapped in different geometry in such a way that no CT takes place.

As mentioned above, the shorter decay time value (τ_1) decreases with increase in the temperature range 240–294 K. A plot of the reciprocal of the decay time value with temperature (Table 3) shows an Arrhenius type behavior (Fig. 5) i.e.,

$$1/\tau_1 = \mathrm{A}e^{-E/kT} \tag{4}$$

where the activation energy (E) of the non-radiative process has been obtained to be 5.07 K cal/mol. The decrease in the τ_1 value beyond 240 K cannot be attributed to any other process except for an increase in the temperature-dependent non-radiative rate. This is supported by the fact that, the decay curves analyzed across the emission wavelength do

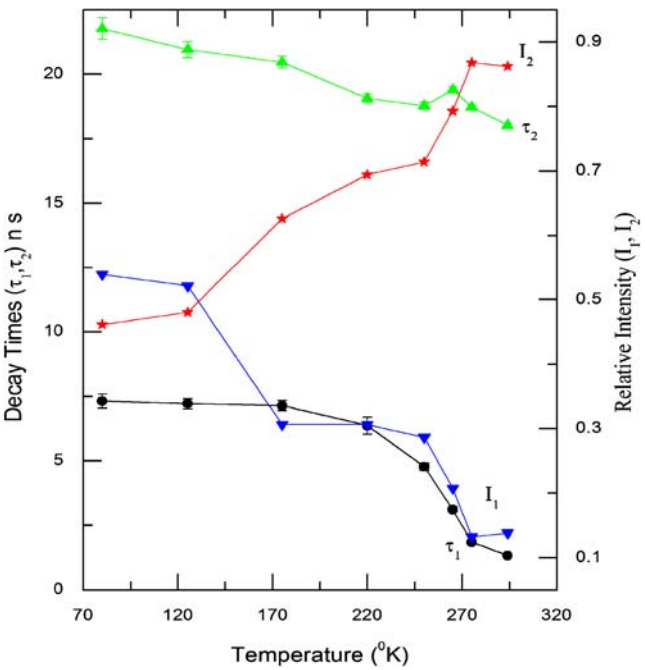

Fig. 4 Curve of fluorescence decay times (τ_1 and τ_2) and relative decay intensities (I_1 and I_2) against temperature of C^{++} in glycerol/water (1:1) system. (λ_{ex}=320 nm λ_{em}=420 nm)

Table 3 Time domain parameters of cinchonine alkaloid in 1 N H_2SO_4 glycerol/water (1:1) system at different temperatures (λ_{ex}=320 nm; λ_{em}=420 nm)

Temperature (K)	τ_1 (ns)	τ_2 (ns)	α_1	α_2	χ^2	$I_1 = \frac{\alpha_1\tau_1}{\alpha_1\tau_1+\alpha_2\tau_2}$	$I_2 = \frac{\alpha_1\tau_1}{\alpha_1\tau_1+\alpha_2\tau_2}$
80	7.32±0.28	21.76±0.42	0.066	0.019	1.16	0.5389	0.4611
125	7.22±0.20	20.95±0.32	0.063	0.020	1.07	0.5205	0.4795
175	7.14±0.20	20.46±0.23	0.053	0.031	1.05	0.3062	0.6263
220	6.36±0.33	19.06±0.17	0.041	0.031	1.19	0.3062	0.6938
250	4.77±0.15	18.77±0.15	0.052	0.033	1.11	0.2859	0.7140
265	3.11±0.10	19.39±0.12	0.057	0.035	1.12	0.2071	0.7928
275	1.85±0.06	18.72±0.09	0.063	0.041	0.94	0.1318	0.8681
294	1.34±0.04	18.02±0.07	0.157	0.073	1.15	0.1379	0.8621

not show any evidence of additional excited state process. Had there been any such process, we should have observed a rise time in the decay plot at least at the red edge of the emission, along with a discontinuity in the decay plot for τ_1 values across the emission wavelength, such a thing has not be observed in this case. Thus, the results point to the existence of two distinct emitting species, having their own characteristic decay rates. Figure 4 also shows a decrease in τ_2 value with increase in temperature which is again related with the increasing temperature-dependent non-radiative processes. An inspection of Table 1 (Fig. 2) shows that τ_2 value (in fluid solution) increases with increase in the emission wavelength. However, τ_1 value remains constant. It appears that the solvent relaxation time τ_r is much larger than τ_1. Hence, before any such solvent relaxation is to take place, the species having shorter decay time return to the ground state by normal fluorescence. However, since τ_2 is large the solvent molecule may find sufficient time to reorient around the excited molecule and hence the emission corresponding to longer decay time species may take place from an unrelaxed as well as relaxed state. Under such condition the τ_2 values show an increase towards the longer emission wavelengths. Various explanations have been given to account for the emitting state above the transition temperature. Kosower et al. [29] have suggested that the emitting state of some arylaminonaphthalene sulphonates is a charge-transfer (CT) state, which arises from a change in geometry, resulting in the phenyl ring residing in the naphthalene plane. Ghiggino et al. [30] reported that a combination of solvent–solute reorientation and a change in geometry within the l-amino substituent of dansyl could result in an emitting state with partial charge-transfer character.

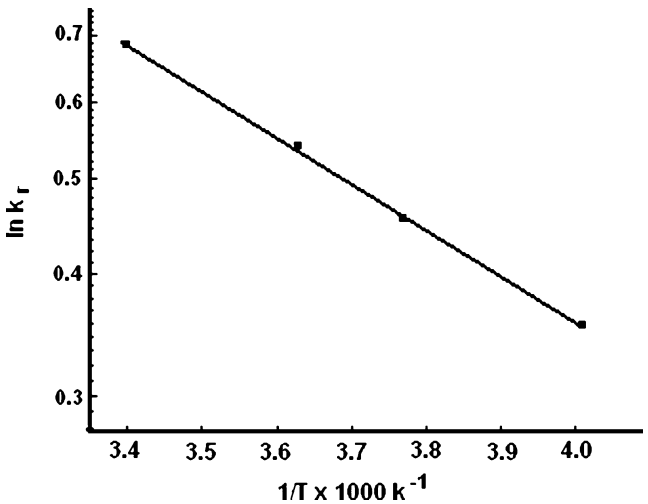

Fig. 5 Curve of ln k_r against 1,000/T (Arrhenius plot)

Time-resolved study

Figure 6 shows the normalized TRES for C^{++} in 1N H_2SO_4 solution of glycerol/water at room temperature. At early time window (0–0.5 ns, 0.5–1.0 ns), the emission with λ_{max}~398 nm is observed, which is dominated by the emission from shorter-lived species. On further increasing the time window, at intermediate delays the spectrum shows a red shift, along with greater FWHM corresponding to emission from both the species. Again further increasing the delay, a continuous shift in emission is observed with almost constant FWHM. Several authors have characterized such TRES in their studies [31, 32]. A simple two state model assumes that the solvent molecules surrounding the excited state fluorophore can exist in only two limiting states: namely the unrelaxed Frank–Condon (FC) state and the relaxed (R) state. In such a model, the solvent relaxation rate k_r is assumed to be fast and the reverse rate is ignored. However, both the relaxed and the unrelaxed states may be directly excited. One of the features of this model is that only two decay time values will be obtained and these values will be constant regardless of the emission wavelength. The two decay time values cannot be associated with either of the two molecular species. These values are a function of both the decay and relaxation rates and under certain circumstances one of the two pre-exponential factors can be negative. However, in the present case of C^{++} a simple two state model fails to describe the relaxation

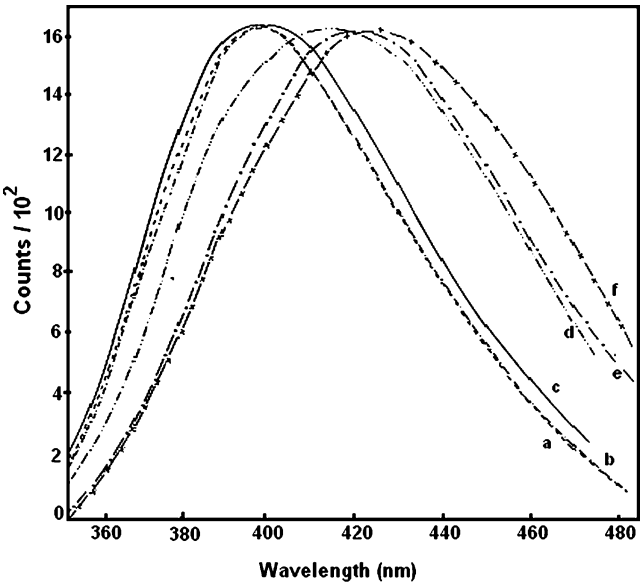

Fig. 6 Peak normalized time resolved emission spectra (TRES) of C^{++} in glycerol/water (1:1) system under the different time windows *a* 0.5 ns, *b* 1.0 ns, *c* 1.5 ns, *d* 6.0 ns, *e* 11.5 ns, *f* 15.0 ns

process. Though τ_1 is practically constant, the longer decay time component τ_2 increases with increasing emission wavelength. Such effects are associated with solvent reorientation process. Since the decay time of the second species is quite large during this time, the solvent molecules may reorient and emission may take place from several partially relaxed species of this state, resulting in the observed broadening is observed. The TRES in Fig. 6 shows that during initial short delays a situation similar to two state relaxation mechanisms is observed. However, at longer delays where the emission due to longer-lived species is dominant the TRES shows a continuous shift with delay time. The TRES at longer time delays have been analyzed using the procedure adopted by DeToma et al. [33] for the continuous shift [34] in time-resolved emission. The solvent relaxation time (τ_r) values have been calculated using the continuum model and adopting the same procedure as discussed by Pant et al. [9], according to which,:

$$\overline{\nu}_m(t) = \overline{\nu}_\infty + (\overline{\nu}_0 - \overline{\nu}_\infty)\exp^{-t/\tau_r} \quad (5)$$

where $\nu_m(t)$ is emission maximum (for Gaussian shape), ν_0 and ν_∞ are the emission maxima at t=0 and t=∞. It is assumed that the shift to lower energy is an exponential function of solvent relaxation time τ_r. The solvent relaxation time (τ_r) has been calculated and the value comes out to be approximately 6 ns. Further, on increasing the C^{++} concentration from 10^{-4} to 10^{-2} M, no significant change in τ_1 is observed, both τ_2 and τ_r are quenched. The concentration quenching in τ_r and τ_2 across the emission wavelength shows nearly similar behavior as observed due to energy migration in QS^{++} [27]. Thus, at lower concentrations the solvent relaxation is higher than energy migration whereas, at higher concentrations the energy migration becomes dominant. This is because, on increasing the concentration, solute–solute interaction increases.

From the above study, it is apparent that two distinct emitting species are present in C^{++}. In a mixture of two fluorophores, if the two spectra overlap each other, the decay associated spectra give the exact nature of the excited state. The decay associated spectra for the shorter and longer decay time components are given in Fig. 7. Here the spectra corresponding to the shorter and longer decay time components are shown by broken curves, and the full curve is the steady state spectrum under identical conditions of excitation wavelength. The shorter decay time component has an emission at around 420 nm while the longer decay time component has a broad band at 450 nm. The decay-associated parameters of C^{++} show that the contribution to the total intensity is approximately 97% because of the shorter-lived species at the blue edge (360 nm). However, the longer decay time component shows an increase in its magnitude towards the red edge of the emission where its intensity contribution is about 60% (at 490 nm). The above results indicated the presence of two distinct emitting species (conformers) with closely lying excited states. The broad band fluorescence emission is due to the presence of these two overlapped species. The time domain behavior suggests that the individual species decay with their own decay rates. Also there is no excited state inter-conversion between these species, as no rising edge could be observed in the emission decay even for longer emission wavelengths. Further, for an excited-state reaction, the decay

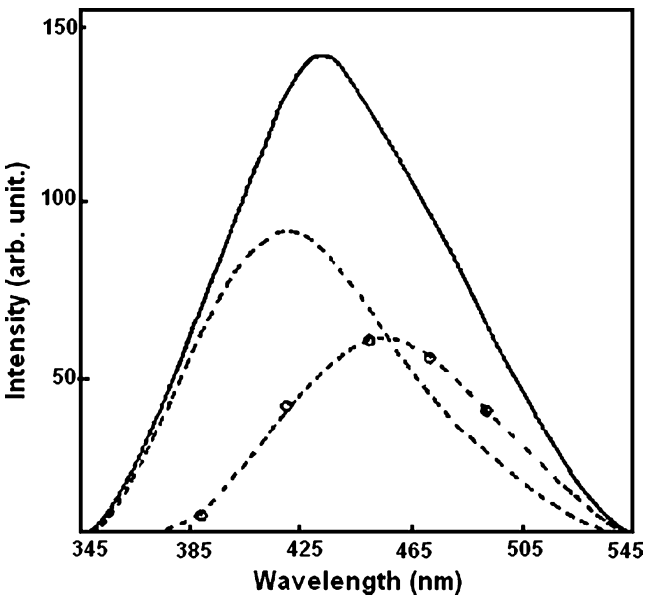

Fig. 7 The decay-associated spectra (DAS) of C^{++} in glycerol/water (1:1) system for the shorter decay time component (– – –), longer decay time component (–○–), (λ_{ex}=320 nm) and steady state spectra under identical conditions of excitation wavelength at 294 K (—)

should show a single-exponential fit at some unique wavelength where the contribution due to emission from a precursor and product overlaps [15, 23]. No such situation has been observed in this case. The decay fits well to a sum of two exponential functions at all emission wavelengths monitored. The changes in the fluorescence characteristics of C^{++} may be due to a change in the relative concentrations of the two distinct species in the ground state. The difference in the decay time values in C^{++} may be due to the difference in the oscillator strengths of this compound. The emission characteristics of C^{++} are similar to those of Qd^{++} and QS^{++}, particularly in respect to the excitation wavelength dependence of emission spectra, EERS and the increase in fluorescence decay times with increasing emission wavelength. However, there are some differences between these two groups of molecules in their fluorescence decay pathways. Although, QS^{++} is also gives two fluorescence decay times in aqueous 1N H_2SO_4 solution at ambient temperature. The variation in the decay times across the emission band resembles a two-state solvent relaxation mechanism [25] with negative amplitude in the region of longer emission wavelength, in contrast, with the decay of C^{++}. The complex behaviors of QS^{++} and Qd^{++} consists of two major relaxation processes: a CT process (from the methoxy group to the quinoline ring) and a solvent relaxation process. The difference between the photophysical behaviors of these two groups of molecules is most probably due to the absence of the methoxy group in C^{++}.

Similar, unusually large solvent relaxation times have been estimated for DANCA [31] in glycerol at 20°C (τ_r~ 1.7 ns) and for protonated ACMA [32] in 90% glycerol τ_r~ 24 ns. The large difference in τ_r values has been explained in the latter compound by the protonation on the acridinium nitrogen site which strongly polarizes solvent molecules in their neighborhoods. In neutral ACMA, the τ_r value decreases to 1.0 ns under the same conditions. It appears that in the systems studied by us, the presence of long solvent reorientation time is influenced by the supplementary interactions between the protonated probe molecule and polar solvent molecules, besides the usual dielectric relaxation time of the solvent molecule similar to the case of protonated ACMA. In our time-resolved experiments, the time resolution was not sufficient to be able to probe the ultra-fast time components of water solvation. Using ultra-fast time-resolved experimental techniques [32], the solvation of water has been shown to be ultra-fast with an inertial solvation time component of less than 100 fs, contributing 70% to the total solvation energy and two slower diffusive sub-picosecond time components. However, we believe that the nanosecond time component resolved here using the dynamic Stocks shift measurements is a slowed down (due to the strong interactions of the SO_4^- ions present in the solution with the C^{++} molecules) diffusive time component of water solvation. There are several reports about the slower solvation time components of water in the presence of the ions in solution [35–39]. Molecular dynamics calculations and experimental data have shown slower solvation dynamics in concentrated ionic solutions than in bulk water. The interactions of water with specific cations influence the water mobility. Impey et al. [35] contrasted the interaction of water with Na^+ and K^+. Their calculations showed the residence time of water in the solvation shell around Na^+ is about twice that for water next to K^+. Their calculations also showed that residence times around divalent cations can be nanoseconds or longer. Guardia and Padro [36] calculated water interacting with Na^+ and have reported longer residence time of 38 ps. Wang and Tominaga [37] have used low frequency Raman spectroscopy to measure the solvent response of ionic solutions, including NaCl, KCl and $CaCl_2$ salt solutions. Their results

Table 4 Quenching of fluorescence decay times of cinchonine in glycerol/water system by chloride ion at 294 K (λ_{ex}=320 nm)

NaCl (M)	λ_{em} (nm)	τ_1 (ns)	τ_2 (ns)	χ^2	τ_0/τ_1	τ_0/τ_2
0.000	390	0.88±0.01	17.91±0.09	1.03	1.00	1.00
0.005		0.81±0.01	11.95±0.33	1.008	1.08	1.36
0.010		0.83±0.01	10.57±0.28	0.962	1.06	1.70
0.020		0.76±0.01	7.68±0.30	0.908	1.15	2.33
0.040		0.71±0.01	5.02±0.29	0.929	1.23	3.56
0.000	420	0.94±0.03	18.70±0.07	1.23	1.00	1.00
0.005		0.91±0.01	13.57±0.23	0.971	1.04	1.33
0.010		0.88±0.01	11.29±0.17	1.057	1.06	1.66
0.020		0.79±0.01	8.31±0.14	0.993	1.19	2.25
0.040		0.73±0.01	5.41±0.12	0.849	1.28	3.46
0.000	470	0.86±0.01	19.70±0.15	1.194	1.00	1.00
0.005		0.83±0.01	14.99±0.11	1.029	1.03	1.31
0.010		0.82±0.01	12.31±0.11	1.104	1.05	1.60
0.020		0.76±0.01	8.99±0.09	1.061	1.13	2.18
0.040		0.69±0.01	5.82±0.08	1.382	1.25	3.34

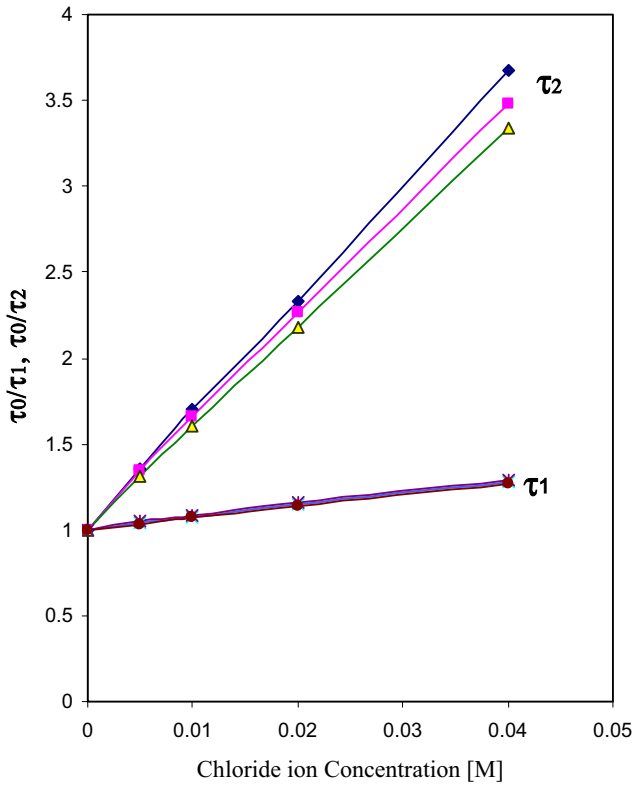

Fig. 8 Stern–Volmer curve of decay times (τ_2 and τ_1) of C^{++} against different concentrations of NaCl: 0.00, 0.005, 0.01, 0.02, and 0.04 M in glycerol/water (1:1) system. The emission wavelength monitored at λ_{em}=390 nm (*blue color*; –□–), 420 nm (*red color*; –Δ–) and 470 nm (*yellow color*; –○–) respectively (λ_{ex}=320 nm)

showed that the ions in solution cause relaxation times to become progressively longer with increasing concentration. Obst and Bradaczek [38] found that the interaction of Ca^{2+} ions was significantly stronger than the interaction of alkali ions with water. Using a combined quantum mechanical/molecular mechanical dynamics calculation, Tongraar et al. [39] have shown that the translational, librational and vibrational motion of water near Ca^{2+} is perturbed due to ion water interactions.

Fluorescence quenching

In fluorescence quenching experiment of C^{++} in glycerol/water (1:1) system by chloride (Cl^-) ion, shows that both fluorescence intensity as well as decay time of C^{++} ion, decreases with increase in Cl^- ion concentration. The fluorescence decay time parameters of C^{++} under different chloride (Cl^-) ion concentration at different emission wavelength are given in Table 4. The quenching follows Stern–Volmer relation:

$$\frac{\tau}{\tau_0} = 1 + K_q \tau_0 [Q] \tag{6}$$

where $[Q]$ is the concentration of the quencher (Cl^-). Figure 8 shows the plots of τ_0/τ_1 and τ_0/τ_2 vs chloride ion concentration. (τ_0 values are taken as the value of respective decay time in absence of quencher ion). Dynamic type fluorescence quenching is observed although, unlike QS^{++} and Qd^{++}, no rise time is observed at the red edge of the emission. The Stern–Volmer quenching constant ($K_{SV}=K_q\tau_0$) values have been calculated for τ_1 and τ_2 using the above relation. For lower decay time species, the K_{SV} is approximately 6.58 M^{-1}, while for longer decay time species it is nearly ten fold higher i.e. approximately 66.34 M^{-1} (measured at 470 nm) suggesting that the longer decay time τ_2 species is more prone to Cl^- ion quenching. The fluorescence quenching constant K_q value (calculated from Eq. 6) for emission wavelength 390 nm, 420 nm and 470 nm are 3.7 $M^{-1}S^{-1}$, 3.2 $M^{-1}S^{-1}$ and 2.9 $M^{-1}S^{-1}$ respectively. It shows similar behavior of fluorescence quenching reported by Pant et. al. [11] for QS^{++}. It is interesting to note that at a Cl^- ion concentration 0.04 M, the τ_2 value approaches a constant value ($\tau_2 \sim 5.6$ ns) across the emission wavelength (not shown here). In chloride quenched C^{++} in aqueous acidic solution (at 0.04 M NaCl concentration) the solvent relaxation rate is found to be much faster than in unquenched C^{++} ($\tau_2 \sim 1$ ns). The relative quenching by Cl^- ion is more towards red side (470 nm) as compared to the blue edge (390 nm) (Fig. 8). This suggests that the longer wavelength emission has a charge transfer character. A decrease in the value of τ_2 and its constancy across the emission wavelength for quenched C^{++} is in agreement with the lower value of τ_r. The effect of Cl^- ion quenching on the solvent relaxation rate of the longer-lived species further supported the charge transfer nature of the long lived species. At higher concentration of chloride ion quenching is the dominant process and effect of solvent relaxation is absent. Similar effect of differential Cl^- ion quenching were observed in QS^{++} and $6MQ^{++}$ cation [9–12].

Conclusions

The steady state and time dependent fluorescence studies of C^{++} as a function of temperature clearly point to the existence of two distinct emitting species having their own characteristic decay rates. The shorter-lived species shows usual temperature dependence with increasing non-radiative deactivation at higher temperatures. While, the longer-lived species shows features resembling to excited state solvent relaxation process with a large solvent relaxation time $\tau_r \sim$ 6 ns. Following, Ghiggino et al. [30] and Pant et. al. [9], we propose two cooperative relaxation mechanisms to account for the temperature dependence of the fluorescence spectra: a solvent relaxation mechanism (which is a large amplitude solute–solvent reorientation mechanism in fluid media) and a relaxation associated with intramolecular motion in the C^{++} molecule itself. The temperature variation at 200 K pro-

vides evidence for a change in nature of the emitting state in C^{++}. The low-lying closely-spaced $\pi\pi^*$ states of the main chromophore are L_a and L_b states. The absorptions corresponding to these transitions have similar extinction coefficients and interact with each other. They seem to have considerable charge-transfer character. It has been suggested that both of the relaxation mechanisms mentioned above increase the charge transfer character in the excited state. The excited state reorganization or geometry change as proposed by Kosower et al. [29] may result in a charge transfer state. The edge excitation red shift (EERS) of emission maximum, emission wavelength dependence of fluorescence decay times and the time dependent fluorescence Stokes shift (TDFSS) are known to occur due to solvent relaxation process.

Further, the fluorescence quenching of C^{++} follows the Stern–Volmer relation. The species emitting in the lower energy side, having longer decay time is sensitive to chloride ion and concentration quenching. However, the two emissions τ_1 and τ_2 are differentially quenched with the result that the spectra shift to the blue and the quenching is more pronounced for the longer wavelength emission. This behavior can be understood on the basis of excited state solute–solvent interaction. The spectral shift is a result of the reorientation of the solvent dipoles around the changed dipole moment of the fluorophore. The initial emission will be from the FC state and the relaxed state will emit in the long wavelength region. There will be several intermediate solute–solvent configurations emitting between the FC and relaxed states even at low temperature.

Acknowledgment One of the authors (HM) is thankful to CSIR and DST, New Delhi, India for the financial assistance. Dr. Supriya Tilvi, MBU, IISc, Bangalore is acknowledged for the critical reading of the manuscript. The authors are thankful to DST and CSIR, New Delhi, India for the financial assistance. The authors are also thankful to the reviewers for their helpful comments.

References

1. Franz MH, Röper S, Wartchow R, Hoffmann HMR (2004) The first and second cinchona rearrangement. Two fundamental transformations of alkaloid chemistry. J Org Chem 69:2983–2991
2. Hoffmann HMR, Frackenpohl J (2004) Recent advances in cinchona alkaloid chemistry. Eur J Org Chem 21:4293–4312
3. Kold HC, Van Nieuwenhze MS, Sharpless KB (1994) Catalytic asymmetric diydroxylation. Chem Rev 94:2463–2547
4. Braje WM, Wartchow R, Hoffmann HMR (1999) Structure and mechanism in cinchona alkaloid chemistry: overturning a 50-year-old misconception. Angew Chem Int Ed Engl 38:2539–2543
5. Yu D, Sujuki M, Xie L, Moriss-Natschke SL, Lee KH (2003) Recent progress in the development of coumarin derivatives as potent anti-HIV agents. Med Res Rev 23:322–345
6. Hutzter JM, Walker GS, Wienkers LC (2003) Inhibition of cytochrome P450 2D6: structure–activity studies using a series of quinidine and quinine analogues. Chem Res Toxicol 16:450–459
7. Spikes JD (1998) Photosensitizing properties of quinine and synthetic antimalarials. J Photochem Photobiol B Biol 42:1–11
8. Oh EC, Kim Y (1988) The Pfeiffer effect of $[Co^{II}(acac)_2$ (diamine)] with Cinchona alkaloid in some organic solvents. Bull Korean Chem Soc 9:355–359
9. Joshi HC, Upadhyay A, Mishra H, Tripathi HB, Pant DD (1999) Edge excitation red shift and microenvironmental effects on the photophysics of quinine bisulphate. J Photochem Photobiol A Chem 122:185–189
10. Pant S, Tripathi HB, Pant DD (1995) Solvent polarity and viscosity effect on the fluorescence spectrum and excited state decay time of quinine dication. J Photochem Photobiol A Chem 85:33–38
11. Demchenko AP (2002) The red-edge effects: 30 years of exploration. Luminescence 17:19–42
12. Pant D, Tripathi UC, Joshi GC, Tripathi HB, Pant DD (1990) Photophysics of doubly-charged quinine: steady state and time-dependent fluorescence. J Photochem Photobiol A Chem 51:313–325
13. Pant D, Tripathi HB, Pant DD (1990) Photophysics of protonated 6-methoxyquinoline: steady state and time-dependent fluorescence. J Photochem Photobiol A Chem 54:239–249
14. Itoh K, Azumi T (1975) Shift of the emission band upon excitation at the long wavelength absorption edge. II. Importance of the solute–solvent interaction and the solvent reorientation relaxation process. J Chem Phys 62:3431–3438
15. O'Connor DV, Meech SR, Phillips D (1982) Complex fluorescence decay of quinine bisulphate in aqueous sulphuric acid solution. Chem Phys Lett 88:22–26
16. Bakhshiev NG (1962) Universal molecular interactions and their effect on the position of the electronic spectra of molecules in two component solutions. II. Phthalimide derivatives (liquid solutions). Opt Spektrosk 12:582–587
17. Bakhshiev NG (1962) Universal intermolecular interactions and their effect on the position of electron spectra of molecules in dissolved two-component solutions. VI. Dipole moments and the structure of molecules of some derivatives of phthalimide in the ground and the first excited electron states. Opt Spektrosk 13:192–201
18. Bakhshiev NG, Mazurenko YT, Peterskaya IV (1966) Luminescence decay in various regions of the luminescence spectrum of molecules in viscous solvents. Opt Spektrosk 21(5):550–554
19. Bakhshiev NG, Klochkov VP, Neporent BS, Cherkasov AS (1962) Absorption and fluorescence of the vapor of anthracene and its derivatives. Opt Spektrosk 12:582–587
20. Bakhshiev NG, Gularyan SK, Dobretsov GE, Kirillova YA, Svetlichny VY (2006) Solvatochromism and solvatofluorochromism of the intramolecular charge transfer and of 4-dimethylaminochalcone in the electronic spectra of its solutions. Opt Spectrosc 100:700–708
21. Azumi T, Itoh K, Shiraishi H (1976) Shift of emission band upon the excitation at the long wavelength absorption edge. III. Temperature dependence of the shift and correlation with the time dependent spectral shift. J Chem Phys 65:2550–2555
22. Ikeyama T, Azumi T, Murso T, Yamazaki I (1983) Shift of emission band upon excitation at the long-wavelength absorption edge. Time-dependent fluorescence shift of a fluid ethanol solution of 6-methoxyquinoline. Chem Phys Lett 96:419–421
23. Meech SR, Phillips D (1983) Photophysics of some common fluorescence standards. J Photochem 23:193–217
24. Mishra H (2002) Photoinduced electronic excited state relaxation and proton transfer phenomena in some hydrogen bonded molecules. Ph.D. Thesis, Kumaon University, Nainital, India
25. Pant S, Pant D, Tripathi HB (1993) Photophysics of the dications of cinchonine and cinchonidine. J Photochem Photobiol A Chem 75:137–149
26. Liu Y, Yang YW, Zhang HY, Hu BW, Ding F, Li CJ (2004) Diastereoisomer selective inclusion of Cinchona alkaloids with a modified β-cyclodextrin: fluorescent behaviour enhance by chiral teather binding. Short communication. Chem Biodivers 1:481–488

27. Mishra H, Pant D, Pant TC, Tripathi HB (2006) Edge excitation red shift and energy migration in quinine bisulphate dication. J Photochem Photobiol A Chem 177:197–204
28. Strickler S, Berg RA (1962) Relationship between absorption intensity and fluorescence decay time of molecules. J Chem Phys 37:814
29. Kosower EM, Dodiuk H, Kanety H (1978) Intramolecular donor–acceptor system. 4. Solvent effects on radiative and nonradiative processes for the charge-transfer states of *N*-arylaminonaphthalenesulfonates. J Am Chem Soc 100:4179–4188
30. Ghiggino KP, Lee AG, Meech SR, O'Connor DV, Phillips D (1981) Time-resolved emission spectroscopy of the dansyl fluorescence probe. Biochemistry 20:5381–5389
31. Bismuto E, Jameson DM, Gratton E (1987) Dipolar relaxations in glycerol: a dynamic fluorescence study of 4-[2′-(dimethylamino)-6′-naphthoyl]cyclohexanecarboxylic acid (DANCA). J Am Chem Soc 109:2354–2357
32. Sun JS, Rougee M, Delarue M, Garestier TM, Helene C (1990) Solvent relaxation around excited 2-methoxy-6-chloro-9-aminoacridine in aqueous solvents. J Phys Chem 94:968–977
33. DeToma RP, Ester JH, Brand L (1976) Dynamic interaction of fluorescence probes with the solvent environment. J Am Chem Soc 98:5001–5007
34. Jimenez R, Fleming GR, Kumar PV, Maroncelli M (1994) Femtosecond solvation dynamics of water. Femtosecond solvation dynamics of water. Nature 369:471–473
35. Impey W, Madden PA, Mcdonald IR (1983) Hydration and mobility of ions in solution. J Phys Chem 87:5071–5083
36. Guardia E, Padro JA (1990) Molecular dynamics simulation of single ions in aqueous solutions: effects of the flexibility of the water molecules. J Phys Chem 94:6049–6055
37. Wang Y, Tominaga Y (1994) Dynamical structure of water in aqueous electrolyte solutions by low-frequency Raman scattering. J Chem Phys 101:3453–3458
38. Obst S, Bradaczek H (1996) Molecular dynamics study of the structure and dynamics of the hydration shell of alkaline and alkaline-earth metal cations. J Phys Chem 100:15677–15687
39. Tongraar A, Liedl KR, Rode BM (1997) Solvation of Ca^{2+} in water studied by Born–Oppenheimer ab initio QM/MM dynamics. J Phys Chem A 101:6299–6309